COMMUNICATION

Revelation of Intertwining Organic and Inorganic Fractal Structures in Polymer Coatings

A. E. Hughes, A. Trinchi, F. F. Chen, Y. S. Yang, I. S. Cole, S. Sellaiyan, J. Carr, P. D. Lee, G. E. Thompson, and T. Q. Xiao*

One of the most complicated challenges in materials science today is understanding the nature and distribution of networks within materials. This understanding can enable materials to be designed for a broad range of applications spanning drug delivery in pharmaceuticals,[1] extraction from minerals,[2] CO_2[3] and H_2[4] storage materials, bioscaffolds[5] composite materials [6] and structural integrity and self healing in polymers [7,8] to name a few. Characterising the 3D spatial distribution of networks is therefore a first step in using these networks to make new and improved materials. [2b,9,10] Here, we combine the use of synchrotron-based computed tomography (CT) and scanning electron microscopy-ultramicrotomy to study the distribution of micrometer-sized inorganic particles within a polymer matrix. Unlike small angle X-ray scattering (SAXS), which is often used to measure the average properties of weakly period systems, typically at the 5 to 25 nm scale, analysis of the CT data offers an avenue to measure substructures within the inorganic/polymer composite on the micrometer to hundreds of micrometers scale. Specifically, this approach allows the identification of different components, determination of their spatial distribution and properties such as their fractal dimension. The system we have chosen consists of strontium chromate in an epoxy-polyamine polymer matrix. We demonstrate that the inorganic particles distributed in a polymeric matrix can form independent, but interpenetrating clusters of varying size and fractal dimension with the largest having a fractal dimension of 2.36. Because the strontium chromate is soluble, it can act as a template for the formation of void clusters with the same characteristics as the original strontium chromate ($SrCrO_4$) clusters.

A. E. Hughes, A. Trinchi, F. F. Chen,
Y. S. Yang, I.S. Cole
CSIRO Materials Science and Engineering
Private Bag 33, Clayton 3169, Australia
E-mail: tony.hughes@csiro.au
S. Sellaiyan
University of Tsukuba Tandem Accelerator Complex
University of Tsukuba
Tennodai 1-1-1, Ibaraki 305-8577, Japan
J. Carr, P. D. Lee, G. E. Thompson
School of Materials
The University of Manchester
Manchester M13 9PL, England, UK
T. Q. Xiao
Shanghai Institute of Applied Physics
Chinese Academy of Sciences
Shanghai 201800, P. R. China

DOI: 10.1002/adma.201400561

These clusters (void or inorganic phase) can act as either reservoirs for drug delivery, inhibitors in self-healing coatings or mechanical reinforcement in polymers. From the authors' perspective this system is of great importance since it represents a model for protective coatings. The release of $SrCrO_4$ inhibitor from epoxies is not well understood and the discovery of clusters of particles and the possibility of voids created through the dissolution of the cluster represents a significant scientific breakthrough for coatings and other applications as indicated earlier. We have devised metrics that can be used to characterize the clusters and ultimately to control their design.

While there are a few reports on the application of CT to the study of micrometer-sized inorganic phase distributions within polymers,[11] this is largely an unexplored field. In this letter we combine X-ray CT and a new SEM-based sectioning technique called serial block face scanning electron microscopy (SBFSEM)[12] to investigate the 3D distribution of inorganic particles ($SrCrO_4$) in a polymer (epoxy-polyamine matrix). The combination of these two techniques provides spatial information covering four orders of magnitude in scale from 50 nm to 500 μm.

CT volume reconstructions of the sample showed three distinguishable regions comprising the epoxy resin which included regions of low (green) and normal (blue) density volumes (LDE and NDE respectively) and $SrCrO_4$ particles (red) as shown in the full section in **Figure 1**(a). The least-square optimised segmentation approach used here relies on differentiating the individual components on the basis of their linear absorption coefficients, which is derived from their composition. The label "normal" has been used for voxels that match the linear absorption coefficient for the pure epoxy. The LDE is about one-third, implying that it has a lower density. It should be noted that the sample is a long slither, and its outline is of irregular shape. The 3D distribution of the $SrCrO_4$ particles and the LDE are revealed more clearly when the NDE component is removed (Figure 1(b)). However, the image of the total volume of the either the LDE or the $SrCrO_4$ particles does not give any indication of the distribution of structures within this phase.

To investigate these structures, a 3D clustering algorithm, consisting of target phase binarisation and nearest neighbour labelling[13] was developed for the voxels. The CT process divides the total volume of the sample into unit sub-volumes called voxels, which form a 3D lattice. A cluster is defined as a group of neighbouring voxels of the same type of composition. It is important to note that the clustering algorithm does not provide any information of how many $SrCrO_4$ *particles* are involved in cluster formation, it only counts the voxels. For the

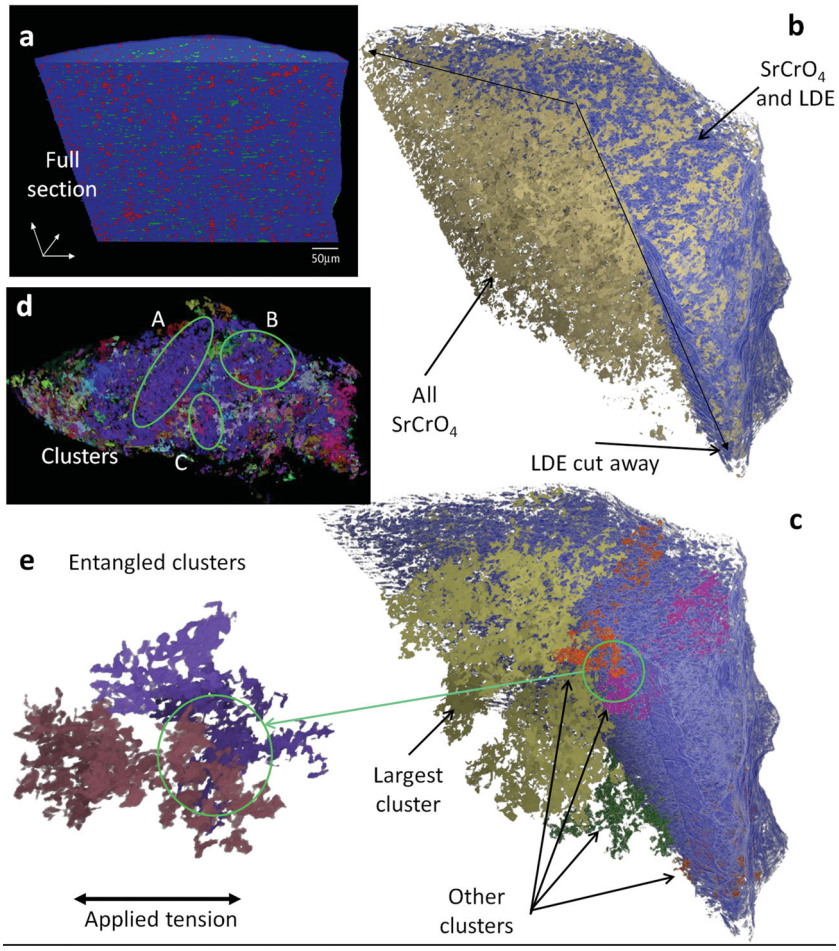

Figure 1. Embedded Fractal Clusters: (a) section through composite containing $SrCrO_4$ (red) embedded in an epoxy matrix with two densities nominated as low density or LDE (green) and normal (blue); (b) 3D reconstruction of LDE (partially cut away) and all the $SrCrO_4$ particles; (c) 3D reconstruction of LDE (partially cut away) and the five largest $SrCrO_4$ clusters; (d) View of all clusters (rendered in different colours) with the largest cluster in blue. A, B, C indicate three different regions of the largest cluster; (e) entanglement of clusters: if tension is applied to the materials then the clusters provide a mechanical resistance improving the shear properties.

LDE, the concept of individual particles is not relevant since it comprises isolated volumes of lower density. For a 3D simple cubic lattice, a voxel can have 6, 18, or 26 neighbours as defined by sharing a common face, line or corner respectively. Often, for real systems, the 26 next-nearest-neighbour connection is used since particles that have a common corner could also have some degree of interaction . For example, when considering transport properties such as with drug delivery, gas release or uptake, liquid transport, or inhibitor release then the 26 nearest neighbour rule will be the most relevant. Here, the 6-neighbour rule was used for calculating fractal dimension and the 26-neighbour rule for calculating cluster statistics (number of clusters and size distribution). Cluster labelling was performed by assigning the same label to any occupied nearest neighbour voxel. If all neighbours were unlabelled, then a new cluster was started. For visualisation, different clusters were rendered in different colours as shown for all clusters in Figure 1(d) and for the five largest clusters in the "cutaway from the LDE" in Figure 1(c) which give an overview of the inter-relationship between the two.

From the colour coding it is evident that there are numerous $SrCrO_4$ clusters with a range of sizes; in fact, using the 26-neighbour rule, there are 9000 clusters with the largest having a volume of 875393 μm^3, constituting 3.37% of the total $SrCrO_4$ volume. As might be expected, the number of clusters is higher with the 6-neighbour rule since voxels with touching corners are not counted as part of the same cluster. Not surprisingly the 26-neighbour rule produces the largest cluster size.

From a broader materials perspective, the clusters displayed in Figure 1 can be considered as an inorganic phase dispersed within a polymer for mechanical reinforcement, or as a soluble template which can form a void network, since the $SrCrO_4$ can be dissolved from the epoxy polyamine polymer.[14] The normalised frequency distribution of cluster sizes is dominated by small clusters (**Figure 2**(a)). However, the largest 100 clusters (of 9000 clusters) constitute around 46% of the total cluster volume. The fractal dimension for the five largest clusters was determined from the gradient of Log (M) versus Log (*L*) (Figure 2(b)), and found to be around 2.3. From Figure 2(b), the maximum linear dimension of the cluster (L_{max}) can be estimated from the point where Log (M) ceases to increase as Log (*L*) increases (region highlighted in red). The largest cluster has a characteristic dimension of ~ 300 μm and the next four largest clusters are ~100 μm. For a cluster with homogeneous density it is expected that Log (M) increases linearly with Log (*L*); however, the clusters observed here show considerable deviation from linearity in the region highlighted in grey with a characteristic length scale labelled L_I. This is because large parts of the cluster are separated by lower density regions of *$SrCrO_4$ within that cluster*, but it may be filled with $SrCrO_4$ from other clusters. Thus L_I represents a scale at which cluster interpenetration occurs and has an influence on the mechanical properties. Computer simulations by Seguardo et al.[15] showed that clustering of particles within composites can play an important role in defining the mechanical properties of materials. They found that particle clustering had its maximum influence at intermediate concentrations where clusters interpenetrated each other introducing a higher flow stress than the polymer matrix. At higher particle density, mechanical properties were dominated by the second phase and at lower densities the properties were dominated by the polymer matrix. Interpenetration is demonstrated in Figure 1(d), where three high density $SrCrO_4$ regions (A, B, C) in the largest cluster are separated by low density regions of $SrCrO_4$ *within* the cluster. Thus, these parameter(L_{max} and L_I), can be used as tools to characterise the clustering and interpenetration of distributed

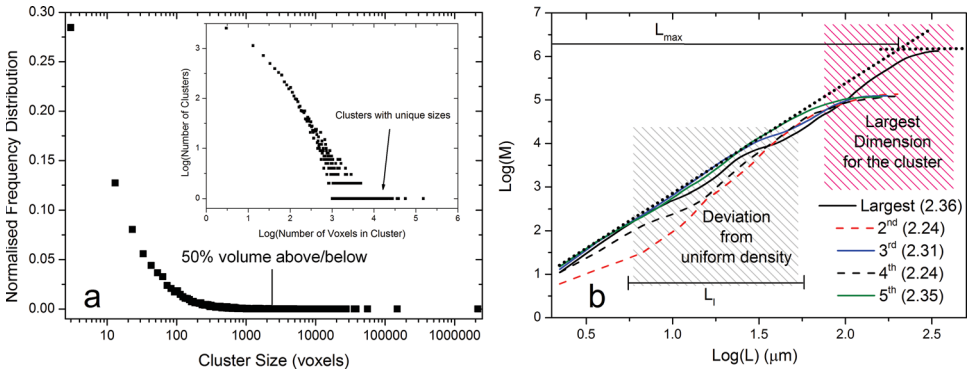

Figure 2. Cluster Statistics: (a) frequency distributions for the $SrCrO_4$ clusters: NB the cluster size scale is a log scale; there is a low frequency of large clusters. The 50% volume line marks the 50% dividing line of the total volume of $SrCrO_4$ is above or below this point. The inset shows the log-log plot of the same distribution but better highlights the larger clusters; (b) variation of Log (M) with Log (*L*) for five largest clusters. The gradient of each line is the fractal dimension for the clusters in brackets. L_{max} marks the largest cluster size and L_I the scale where entanglement occurs. Numbers in brackets are the fractal dimension.

phases in a parent material. In addition the LDE is a second network with the largest cluster having a fractional dimension of about 2.23. It may influence the mechanical properties, since, if it has a lower level of cross-linking, it might be expected that its mechanical properties are inferior to the rest of the epoxy and may provide sites for shear deformation. Interpenetration of two of the largest clusters is shown in Figure 1(e) along with their entangled region highlighted in green.

From a transport perspective, in percolation theory, study of the behaviour of connected clusters in a random distribution has focused on critical phenomena and scaling laws.[16] Theoretically, if the particle density approaches the percolation threshold, then the percolating clusters may have a non-integer fractal dimension.[16,17] The fractal dimension of random-generated percolating clusters at the critical point is approximately 2.5 in three-dimensional space.[16] This implies that the dependence of mass (*M*) to length (*L*) changes from a Euclidean relation ($M \propto L^3$) to a fractal relation ($M \propto L^{2.5}$), i.e., the average density which is normally ($M \sim L^3$) is now ($M \sim L^{2.5}$) with a significant effect on the macroscopic properties as the scale is increased. Transport in such a disordered medium does not follow Fick's law where the mean displacement *R* is proportional to $t^{0.5}$. Stauffer and Aharony[16] demonstrated that the diffusion through a percolation cluster is somewhere between the two extremes of $R \propto t^0$ and $R \propto t^{0.5}$. This of course described the diffusion through a percolating cluster. In our case $SrCrO_4$ clusters connected to the external surface can dissolve directly into solution which contribute mainly at the early release stage and is not influenced by the nature of the percolating cluster. On the other hand, the long-term release behaviour is dominated by the large $SrCrO_4$ clusters and the fractal dimension of the void space left by the dissolved $SrCrO_4$. The large LDE clusters may provide alternative transport paths in addition to the normal epoxy for rapid diffusion of H_2O and other small ions. Indeed, the connections between the LDE and the $SrCrO_4$ may be the first sites of dissolution.

The nature of the connection between different $SrCrO_4$ particles is important from the perspective of both the creation of transport paths and mechanical properties. In the latter case, this is because the mechanical properties of the interfacial regions are likely to be different to both the polymer and the distributed phase. To explore this aspect, SBFSEM was used to characterise the contact points between individual $SrCrO_4$ particles. **Figure 3**(a) shows a series of slices of some $SrCrO_4$ particles highlighting the contact point which is shown in more detail in Figure 3(b). While pixelation limits the ultimate resolution, it appears that the particles are separated by a distance of only one to two pixels which, at a pixel size of 54 nm, represents a distance of 54 to 108 nm. The relationship of the LDE to the $SrCrO_4$ could only be explored using X-ray contrast. As can be seen in Figure 3(c), the $SrCrO_4$ particles/clusters were surrounded by NDE and contacted the LDE only occasionally (see inset). This suggests that potentially faster transport paths through the LDE rarely contact the $SrCrO_4$ directly. It also suggests that volumes with weaker mechanical properties (LDE) reside between clusters and highlight the importance of the cluster structure during mechanical deformation.

Understanding how inorganic materials are distributed within a parent polymeric material will be helpful to designing future materials, and this study has revealed that such inorganic particles can form independent clusters within their polymeric host. These clusters have a range of fractal dimensions with the largest being around 2.3, and transport in such media does not follow Fickian diffusion, which has traditionally been employed to describe species transport in such systems. In addition, we have revealed that volumes of LDE permeate the material and may provide alternative transport paths or represent volumes of inferior mechanical properties, and this provides the opportunity to tune hybrid organic-inorganic systems so as to contain reservoirs for material transport, such as in self-healing coatings or in drug delivery

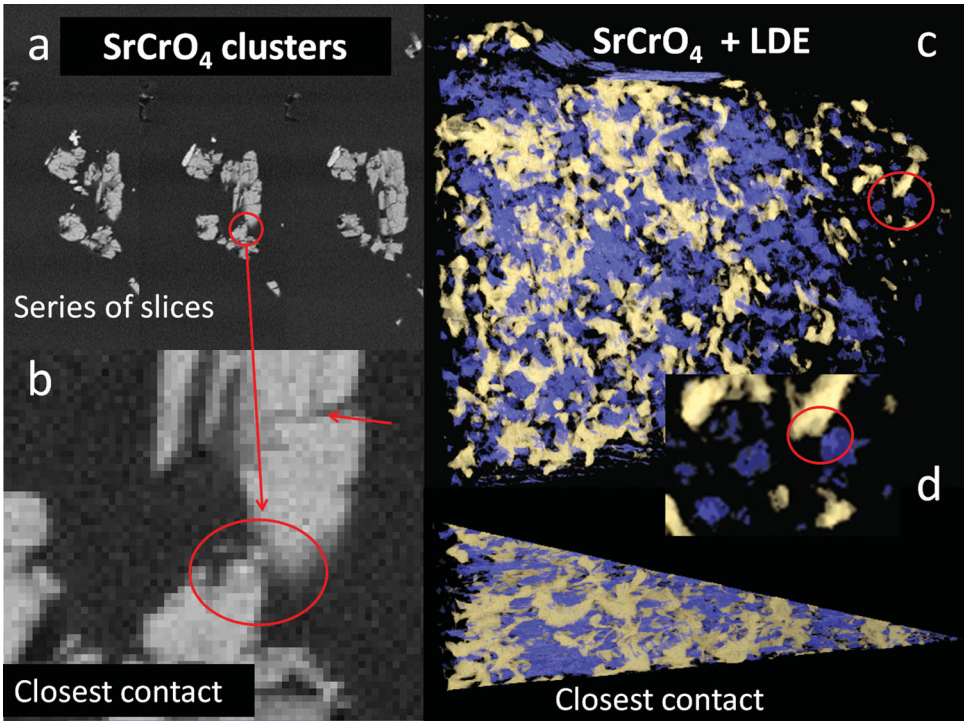

Figure 3. Inter-relationship of $SrCrO_4$ and LDE:. (a) series of 3 slices through a group of $SrCrO_4$ particles highlighting (red circle) where two of the group touch; (b) magnification of the area where they touch; the pixel size is 54 nm; (c) reconstruction of $SrCrO_4$ and LDE in the shape of a wedge as shown in (d). At the right hand side of the wedge individual volumes of each phase can be seen whereas on the left hand side the complexity of the spatial relationship between the two can be seen. Generally, the $SrCrO_4$ does not "touch" the LDE, indicating that it is surrounded by NDE: however, occasionally it does touch, as highlighted by the region within the red circle and magnified in the inset.

Experimental Section

Materials: Epikote 828 (Resolution Performance Product) is a medium viscosity liquid epoxy resin produced from bisphenol A and epichlorohydrin. Hardener 92133 was supplied by Akzo Nobel Aerospace Coating (ANAC). $SrCrO_4$ was obtained from Akzo-Nobel ANAC.

Sample preparation: Samples were prepared by adding the $SrCrO_4$ to the Epikote 828 (1 g). The molar ratio of Epikote, $SrCrO_4$ and hardener was optimized to increase viscosity and to ensure even coating using doctor blades. $SrCrO_4$ (0.5 g) was added to the Epikote (1 g) followed by hardener 92133 (2.2 mL). The constituents were mixed and then allowed to stand (5–10 minutes) at room temperature to thicken, and then coated onto glass microscope slides, resulting in an approximately 100 μm thick film. Films were left to dry overnight at room temperature and then cured at 40 °C for 7 days.

X-ray CT Studies: The X-ray CT projection images were acquired at room temperature and ambient pressure at the Shanghai Synchrotron Radiation Facility (SSRF) BL13W imaging beam-line. A double-crystal monochromator was employed to monochromate the white beam from the wiggler. Projection images were collected at 15.5 keV, with an acquisition time of 2 seconds for each projection. Images were acquired on an Optique Peter X-ray CCD detector which has a native pixel size of 7.4 μm. A 10× optical lens was employed to achieve an effective pixel size of 0.74 μm. A total of 900 projection images was collected with a total sample rotation angle of 180°. In addition, dark-current images were obtained at the beginning and at the end of the scan to account for noise from the CCD. In order to compensate for temporal variations in the flat-field of the beam, the sample was moved out of the X-ray beam and 2 flat-field images were acquired after every 50 projections.

CT slices were reconstructed from the projection images after being normalised with flat-field and dark-current images, subject to Paganin's phase-retrieval using the filtered back-projection method[18] and with ring artefact correction. These processed datasets, containing information of absorption indices were used for further analysis by using the least-square optimised segmentation method,[2b] in which the constituent material phases were spatially resolved using an optimized least squares minimization approach.[2b] Visualization and surface rendering were also undertaken in Drishti.

Serial Block Face Scanning Electron Microscopy: To complement the X-ray CT studies, SBFSEM[12b] was undertaken at the University of Manchester using a 3View facility (see Supporting Information).[12a] Preparation of the samples consisted of embedding the cured polymer in an epoxy resin, which was subsequently ultramicrotomed to produce a tip measuring 50 μm by 300 μm.

This facility implements an environmental scanning electron microscope (ESEM) operating under low vacuum conditions to prevent charging of the non-conductive coating. The ESEM utilises a back-scattered electron (BSE) detector and an electronically actuated, in situ ultramicrotome to perform automated serial sectioning of the sample (using a diamond knife) between low energy BSE scans of the block face. 1000 slices were acquired with dimensions of 1024×1024 pixels; the individual slice thicknesses were 55 nm with a pixel size of 54 nm × 54 nm, producinga 55 μm × 55 μm × 55 μm image.

Supporting Information

Supporting Information is available from the Wiley Online Library or from the author.

Acknowledgements

The authors would like to thank the EPSRC for funding of the LATEST 2 programme Grant, and the Research Complex at Harwell which is partly funded by the EPSRC (EP/102249X/1).

Received: February 4, 2014
Revised: March 27, 2014
Published online: May 2, 2014

[1] a) D. A. Edwards, J. Hanes, G. Caponetti, J. Hrkach, A. BenJebria, M. L. Eskew, J. Mintzes, D. Deaver, N. Lotan, R. Langer, *Science* **1997**, *276*, 1868–1871; b) S. K. Sahoo, V. Labhasetwar, *Drug Discovery Today* **2003**, *8*, 1112–1120.

[2] a) C. H. Arns, F. Bauget, A. Ghous, A. Sakellariou, T. J. Senden, A. P. Sheppard, R. M. Sok, W. V. Pinczewski, J. C. Kelly, M. A. Knackstedt, *Petrophysics* **2005**, *46*, 260–277; b) Y. S. Yang, T. E. Gureyev, M. B. Tulloh, M. B. Clennell, M. Pervukhina, *Measurement Sci.Technol.* **2010**, *21*; c) Y. S. Yang, K. Y. Liu, S. Mayo, A. Tulloh, M. B. Clennell, T. Q. Xiao, *J. Petroleum Sci. Eng.* **2013**, *105*, 76–83; d) H. P. Wang, Y. S. Yang, Y. D. Wang, J. L. Yang, J. Jia, Y. H. Nie, *Fuel* **2013**, *106*, 219–225; e) Y. D. Wang, Y. S. Yang, T. Q. Xiao, K. Y. Liu, B. Clennell, G. Q. Zhang, H. P. Wang, *Int. J. Geosci.* **2013**, *4*, 344–351.

[3] R. Juanes, E. J. Spiteri, F. M. Orr Jr., M. J. Blunt, *Water Resources Res.* **2006**, *42*.

[4] M. Hirscher, B. Panella, B. Schmitz, *Microporous Mesoporous Mater.* **2010**, *129*, 335–339.

[5] J. R. Jones, P. D. Lee, L. L. Hench, *Phil. Trans. R. Soc. A - Mathematical Physical and Engineering Sciences* **2006**, *364*, 263–281.

[6] E. Munch, M. E. Launey, D. H. Alsem, E. Saiz, A. P. Tomsia, R. O. Ritchie, *Science* **2008**, *322*, 1516–1520.

[7] K. S. Toohey, N. R. Sottos, J. A. Lewis, J. S. Moore, S. R. White, *Nat. Mater.* **2007**, *6*, 581–585.

[8] a) E. N. Brown, S. R. White, N. R. Sottos, *J. Mater. Sci.* **2004**, *39*, 1703–1710; b) S. R. White, N. R. Sottos, P. H. Geubelle, J. S. Moore, M. R. Kessler, S. R. Sriram, E. N. Brown, S. Viswanathan, *Nature* **2001**, *409*, 794–797.

[9] a) Y. S. Yang, *Lecture Notes in Information Technology* **2012**, *15*, 198–205; b) F. Tariq, P. D. Lee, R. Haswell, D. W. McComb, *Chem. Eng. Sci.* **2011**, *66*, 5804–5812.

[10] F. F. Chen, Y. S. Yang, *Modelling Simul. Mater. Sci. Eng.* **2012**, *20*.

[11] a) A. Trueman, S. Knight, J. Colwell, T. Hashimoto, E. Koroleva, G. Thompson, in *Annual Conference of the Australasian Corrosion Association 2012*, **2012**, pp. 605–613; b) S. Yang, D. C. Gao, T. Muster, A. Tulloh, S. Furman, S. Mayo, A. Trinchi, in *PRICM 7*, Pts 1-3, Vol. *654-656* (Eds.: J. F. Nie, A. Morton), **2010**, pp. 1686–1689.

[12] a) W. Denk, H. Horstmann, *PLOS Biol.* **2004**, *2*, 1900–1909; b) A. Zankel, B. Kraus, P. Poelt, M. Schaffer, E. Ingolic, *J. Microsc.* **2009**, *233*, 140–148.

[13] L. F. He, Y. Y. Chao, K. J. Suzuki, *IEEE Trans. Image Processing* **2008**, *17*, 749–756.

[14] S. Sellaiyan, A. E. Hughes, S. V. Smith, A. Uedono, J. Sullivan, S. Buckman, *Progr. Org. Coatings* **2014**, *77*, 257–267.

[15] J. Segurado, C. Gonzalez, J. Llorca, *Acta Mater.* **2003**, *51*, 2355–2369.

[16] D. Stauffer, A. Aharony, *Introduction to Percolation Theory*, 2nd ed., Taylor and Francis, London, **1994**.

[17] B. B. Mandelbrot, Freeman, San Francisco, **1982**.

[18] D. Paganin, S. C. Mayo, T. E. Gureyev, P. R. Miller, S. W. Wilkins, *J. Microsc.* **2002**, *206*, 33–40.